*J. Fluid Mech.* (1975), *vol.* 67, *part* 3, *pp.* 583–595
*Printed in Great Britain*



# Prediction of turbulent flow in curved pipes

By S. V. PATANKAR, V. S. PRATAP
AND D. B. SPALDING
Department of Mechanical Engineering, Imperial College, London

(Received 31 May 1974)

A finite-difference procedure is employed to predict the development of turbulent flow in curved pipes. The turbulence model used involves the solution of two differential equations, one for the kinetic energy of the turbulence and the other for its dissipation rate. The predicted total-velocity contours for the developing flow in a 180° bend are compared with the experimental data. Predictions of fully developed velocity profiles for long helically wound pipes are also presented and compared with experimental measurements.

## 1. Introduction

### 1.1. *The problem considered*

Fluid flow in curved ducts is of importance in several engineering applications such as pipe bends, cooling and heating coils, blade passages of turbomachinery, and aircraft intakes. The flow in curved pipes differs from that in a straight pipe principally through exhibiting a 'secondary' flow in planes normal to the main flow (figure 1). Centrifugal forces act at right angles to the main direction of the flow, so that the profile of axial velocity is distorted and the point at which the velocity has its peak is shifted to the outside. The flow is three-dimensional, whereas that in a straight pipe is two-dimensional.

In the present study, the parabolic differential equations governing the curved-pipe flow are solved by the procedure of Patankar & Spalding (1972). In a previous report (1974), the authors studied laminar flow in helical coils; they found that the procedure was quite satisfactory for predicting the flow and heat-transfer characteristics. The present report is an extension of the same numerical procedure for calculation of turbulent flow in curved pipes.

### 1.2. *Past work*

The literature on turbulent flow in curved pipes is quite extensive. Experimental investigations have been carried out by several authors and are summarized by Ito (1959). However, most of the investigators restricted their measurements to bulk quantities like the average friction factor; in a few cases the axial velocity profiles were also measured, namely by Hogg (1968) and Mori & Nakayama (1967). Also, in most of the investigations, only the 'fully developed' flow regime was studied; this occurs when the pipe is helical in form and long enough for the pattern of fluid flow and heat transfer to remain unchanged from one section to the next.

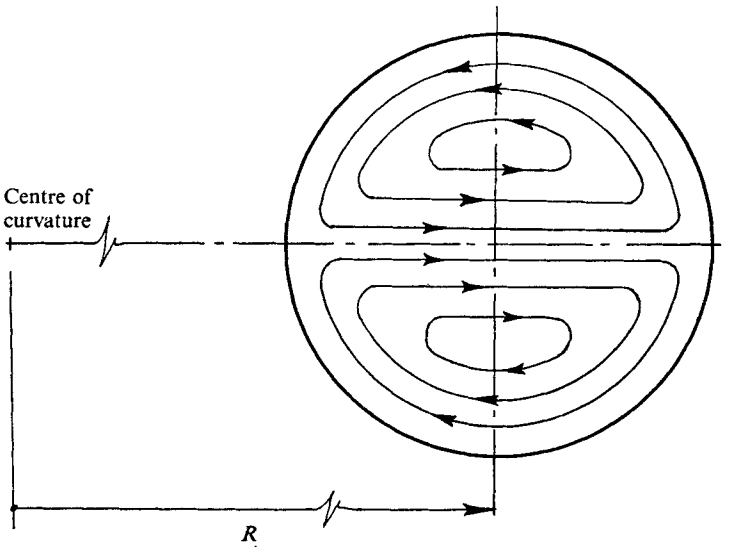


FIGURE 1. Secondary flow pattern.

Rowe (1966), however, presented detailed measurements of stagnation-pressure contours and yaw angles for developing flow in pipe bends for various configurations. He also extended the inviscid-flow theory of Hawthorne (1951) to predict the experimental data. There have as yet been no detailed measurements of the turbulence quantities or of the Reynolds-stress tensor in curved pipes; nor have any theoretical predictions been made.

### 1.3. *Present work*

The success achieved in predicting the laminar-flow phenomena by the method of Patankar & Spalding (1972) encouraged the authors to extend the calculation procedure to the prediction of turbulent flow in curved pipes. The numerical capabilities remain adequate; however, a new difficulty appears, namely that of 'modelling' the turbulence phenomena.

In the first instance, a simple turbulence model of the mixing-length type was used. The predictions using the simple Nikuradse length-scale distribution did not agree satisfactorily with the experimental data for fully developed flow. It was then decided to use a 'two-equation' turbulence model (Launder & Spalding 1972); this necessitates solution of two additional differential equations, one for the kinetic energy of the turbulence and another for a variable relating the length scale and kinetic energy of the turbulence. Such models have been previously used by Ng & Spalding (1972), Rodi & Spalding (1970), Hanjalić (1970) and others.

The present report describes the application of a two-equation turbulence model, in which the two additional variables are the kinetic energy $k$ of the turbulence and its dissipation rate $\epsilon$; an effective viscosity is calculated from $k$ and $\epsilon$, and with the aid of this the Reynolds stresses are related to the velocity gradients. The governing differential equations for the physical situation and the turbulence

model are described in §2. In §3, comparisons are made with experimental results of Rowe (1966) for the developing flow in a 180° bend, and with the data of Hogg (1968) and Mori & Nakayama (1967) for the fully developed flow in a helically wound coil. Friction factors for fully developed flow are also compared with the empirical relation of Ito (1959).

## 2. Mathematical statement of the problem

### 2.1. *Governing equations*

The physical situation illustrated in figure 2 may conveniently be described in the $(r, \theta, \phi)$ co-ordinate system. The flow is treated as parabolic and the diffusion fluxes in the $\phi$ direction together with terms of small order of magnitude are neglected.

The governing differential equations are the $r$ momentum equation

$$\rho\left(U_r\frac{\partial U_r}{\partial r}+U_\theta\frac{\partial U_r}{r\partial\theta}-\frac{U_\theta^2}{r}+\frac{\partial U_r}{R\partial\phi}-\frac{U_\phi^2}{R}\cos\theta\right)$$
$$=-\frac{\partial p}{\partial r}+\frac{\partial\tau_{rr}}{\partial r}+\frac{1}{r}\frac{\partial\tau_{r\theta}}{\partial\theta}-\frac{\tau_{\theta\theta}}{r}+\frac{1}{r}\tau_{rr}-\frac{\tau_{\phi\phi}}{R}\cos\theta+\frac{\tau_{rr}}{R}\cos\theta-\frac{\tau_{r\theta}}{R}\sin\theta, \quad (2.1)$$

the $\theta$ momentum equation

$$\rho\left(U_r\frac{\partial U_\theta}{\partial r}+U_\theta\frac{\partial U_\theta}{r\partial\theta}+\frac{U_rU_\theta}{r}+U_\phi\frac{\partial U_\theta}{R\partial\phi}+\frac{U_\phi^2}{R}\sin\theta\right)$$
$$=-\frac{\partial p}{r\partial\theta}+\frac{\partial\tau_{r\theta}}{\partial r}+\frac{\partial\tau_{\theta\theta}}{r\partial\theta}+\frac{2}{r}\tau_{r\theta}+\frac{r}{R^2}\tau_{\theta\phi}\sin\theta+\frac{\tau_{r\theta}}{R}\cos\theta-\frac{\tau_{\theta\theta}}{R}\sin\theta \quad (2.2)$$

and the $\phi$ momentum equation

$$\rho\left(U_r\frac{\partial U_\phi}{\partial r}+U_\theta\frac{\partial U_\phi}{r\partial\theta}+U_\phi\frac{\partial U_\phi}{R\partial\phi}+\frac{U_\phi}{R}(U_r\cos\theta-U_\theta\sin\theta)\right)$$
$$=-\frac{\partial\bar{p}}{R\partial\phi}+\frac{\partial\tau_{\phi r}}{\partial r}+\frac{\tau_{\phi r}}{R}\cos\theta+\frac{\partial\tau_{\phi\theta}}{r\partial\theta}-\frac{\tau_{\theta\phi}}{R}\sin\theta+\frac{\tau_{\phi r}}{r}. \quad (2.3)$$

Here $U$ represents the velocity and the subscripts $r$, $\theta$ and $\phi$ refer to the corresponding co-ordinate directions. $\rho$ is the density of the fluid (which is assumed uniform throughout the pipe) and $p$ is the cross-stream pressure field.

The $\tau$'s represent the combined laminar and turbulent stresses and will be expressed in terms of the velocity gradients and an effective viscosity. The expressions for these stresses are given in the appendix.

It may be noted that the streamwise gradient of the pressure $\bar{p}$ is 'decoupled' from the cross-stream gradients of the pressure $p$, to make the solutions parabolic. The decoupling was first introduced by Gosman & Spalding (1971); it has been used by Patankar *et al.* (1974), Curr, Sharma & Tatchell (1972) and Sharma & Spalding (1971) and can be regarded as a necessary and well-established practice.

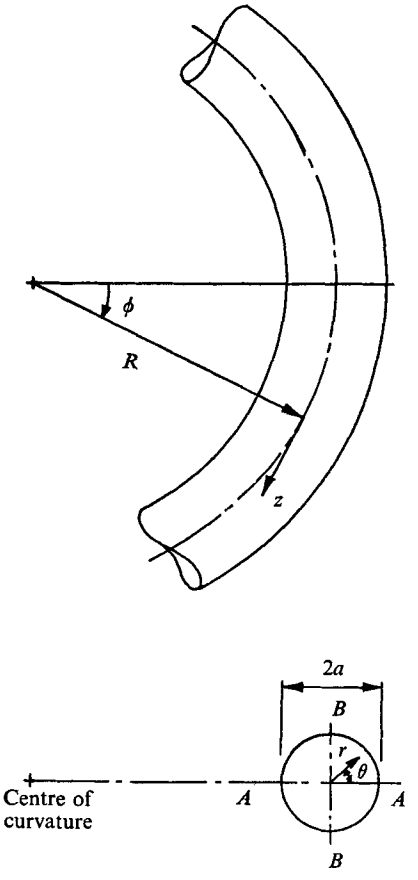


FIGURE 2. The geometry considered.

### 2.2. *The turbulence model*

It is postulated that the Reynolds stresses are related to the mean rate of strain via a turbulent viscosity, the value of which is determined by the local values of the density, turbulent kinetic energy and a length scale. For dimensional homogeneity, the turbulent viscosity $\mu_t$ must be expressed as

$$\mu_t = C'_\mu \rho k^{\frac{1}{2}} l, \tag{2.4}$$

where $C'_\mu$ is a constant at high Reynolds numbers. In the present model, an equation for $k$ is solved and the length scale $l$ is calculated by solving an additional equation for a quantity $\epsilon$; this represents the volumetric rate of dissipation of kinetic energy.

At high Reynolds numbers, $\epsilon$ may be assumed proportional to $k^{\frac{3}{2}}/l$; equation (2.4) may be, therefore, recast as

$$\mu_t = C_\mu \rho k^2/\epsilon, \tag{2.5}$$

where $C_\mu$ is another constant. The governing differential equations for $k$ and $\epsilon$, after neglect of terms of small order of magnitude, are

$$\rho\left(U_r\frac{\partial k}{\partial r}+\frac{U_\theta}{r}\frac{\partial k}{\partial \theta}+\frac{U_\phi}{R}\frac{\partial k}{\partial \phi}\right)=\frac{1}{r}\frac{\partial}{\partial r}\left(\frac{\mu_t}{\sigma_k}r\frac{\partial k}{\partial r}\right)$$
$$+\frac{\mu_t}{R\sigma_k}\left(\frac{\partial k}{\partial r}\cos\theta-\frac{\partial k}{r\partial\theta}\sin\theta\right)+\frac{\partial}{r^2\partial\theta}\left(\frac{\mu_t}{\sigma_k}\frac{\partial k}{\partial\theta}\right)+G-\rho\epsilon, \tag{2.6}$$

$$\rho\left(U_r\frac{\partial \epsilon}{\partial r}+\frac{U_\theta}{r}\frac{\partial \epsilon}{\partial \theta}+U_\phi\frac{\partial \epsilon}{R\partial\phi}\right)=\frac{1}{r}\frac{\partial}{\partial r}\left(\frac{\mu_t}{\sigma_\epsilon}r\frac{\partial \epsilon}{\partial r}\right)$$
$$+\frac{\mu_t}{R\sigma_\epsilon}\left(\frac{\partial \epsilon}{\partial r}\cos\theta-\frac{\partial \epsilon}{r\partial\theta}\sin\theta\right)+\frac{\partial}{r^2\partial\theta}\left(\frac{\mu_t}{\sigma_\epsilon}\frac{\partial \epsilon}{\partial\theta}\right)+C_1\frac{\epsilon}{k}G-C_2\rho\frac{\epsilon^2}{k}. \tag{2.7}$$

In the above equations, $G$ represents the generation of turbulent kinetic energy and can be expressed in terms of the velocity gradients and the turbulent viscosity. The detailed expression for $G$ is given in the appendix. The model contains five empirical constants, which are assigned the following values in accordance with the recommendations of Launder & Spalding (1972):

$$C_\mu = 0{\cdot}09, \quad C_1 = 1{\cdot}47, \quad C_2 = 1{\cdot}92, \quad \sigma_k = 1{\cdot}0, \quad \sigma_\epsilon = 1{\cdot}3.$$

The constants $\sigma_k$ and $\sigma_\epsilon$ are turbulent Prandtl numbers for the diffusive transport of $k$ and $\epsilon$ respectively.

### 2.3. *The wall regions*

In the central region of the flow the gradients of flow properties are usually not very steep; a moderately fine finite-difference grid yields accurate solutions. However, close to solid walls the variations of flow properties are much steeper, thus necessitating an extremely fine grid for their accurate computation. Also, the present form of the turbulence model is valid only for fully turbulent flows; modifications are required to make it applicable to regions where the Reynolds number of the turbulence ($\equiv \rho k^{\frac{1}{2}} l/\mu_l$, where $l \equiv k^{\frac{3}{2}}/\epsilon$) is low.

There are two methods for accounting for the near-wall regions in the numerical methods for computing turbulent flows: the wall-function method and the method of modelling the low-Reynolds-number phenomena. In the present study we adopt the wall-function approach chiefly because of its economy from the viewpoints of both computer storage and computer time.

Wall functions have been proposed and used earlier by several authors including Wolfshtein (1969), Runchal (1969), Ng & Spalding (1972) and Koosinlin & Lockwood (1974). The practices adopted in the present study are described below.

The first step in the method is to locate all the finite-difference grid nodes (except for those representing wall values) in the fully turbulent region. Thus the point $P$ (of figure 3) is located sufficiently far from the wall for the local turbulent Reynolds number $(\rho k^{\frac{1}{2}} l/\mu_l)_P$ to be much greater than unity. It is then assumed that a logarithmic velocity profile prevails in the region between the wall and the node $P$, the expression for the velocity being

$$\frac{U_P}{(\tau/\rho)_w^{\frac{1}{2}}}=\frac{1}{\kappa}\ln\left(\frac{Ey_P(\tau\rho)_w^{\frac{1}{2}}}{\mu_l}\right), \tag{2.8}$$

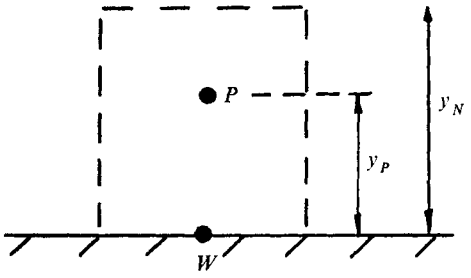


FIGURE 3. Representation of the near-wall region.

where the subscript $P$ indicates values at grid node $P$, $y_P$ is the distance of $P$ from the wall and $\kappa$ and $E$ are the log-law constants. Further, in the uniform-shear-stress layer, the generation and dissipation of $k$ are nearly in balance; it can then be shown that

$$\tau_P = \tau_w = \rho C_\mu^{\frac{1}{2}} k_P. \tag{2.9}$$

By the use of this expression in conjunction with (2.8) the shear stress can be related to the kinetic energy of the turbulence through the relation

$$\tau_P = \frac{\rho\kappa C_\mu^{\frac{1}{4}} k_P^{\frac{1}{2}} U_P}{\ln\{E y_P C_\mu^{\frac{1}{4}} \rho k_P^{\frac{1}{2}}/\mu_l\}}. \tag{2.10}$$

The rate $\epsilon_P$ of dissipation of kinetic energy near the wall is fixed by the requirement that the length scale varies linearly with the distance from the wall; the expression for $\epsilon_P$ is

$$\epsilon_P = C_\mu^{\frac{3}{4}} k_P^{\frac{3}{2}}/\kappa y_P. \tag{2.11}$$

The quantity $k_P$ represents the turbulent kinetic energy near the wall and is calculated from the regular balance equation, the diffusion of energy being set equal to zero. The dissipation term in the kinetic-energy equation is assigned an average value over the control volume for the node near the wall; thus

$$\rho\bar{\epsilon} = \rho \int_0^{y_N} \epsilon \, dy = C_\mu^{\frac{3}{4}} k_P^{\frac{3}{2}} \int_0^{y_N} \frac{1}{\kappa y} dy. \tag{2.12}$$

### 2.4. *Solution procedure*

The above equations, with the appropriate boundary conditions, are solved by a finite-difference procedure, which we describe here only in brief; a complete account is given in Patankar & Spalding (1972). The main feature of the calculation procedure is that the flow properties for one pipe cross-section are deduced from those at an immediately upstream section, as follows.

(1) The average pressure $\bar{p}$ and the pressure distribution $p(r, \theta)$ at the downstream section are guessed.

(2) The momentum equations for the $r$, $\theta$ and $\phi$ directions are then solved to get a first approximation to the downstream velocity distribution.

(3) The mean pressure $\bar{p}$ and the axial velocities are thereupon corrected, by reference to the continuity and linearized longitudinal momentum equations, so as to ensure that the mass flow rate through the downstream section is the same as that through the upstream section.

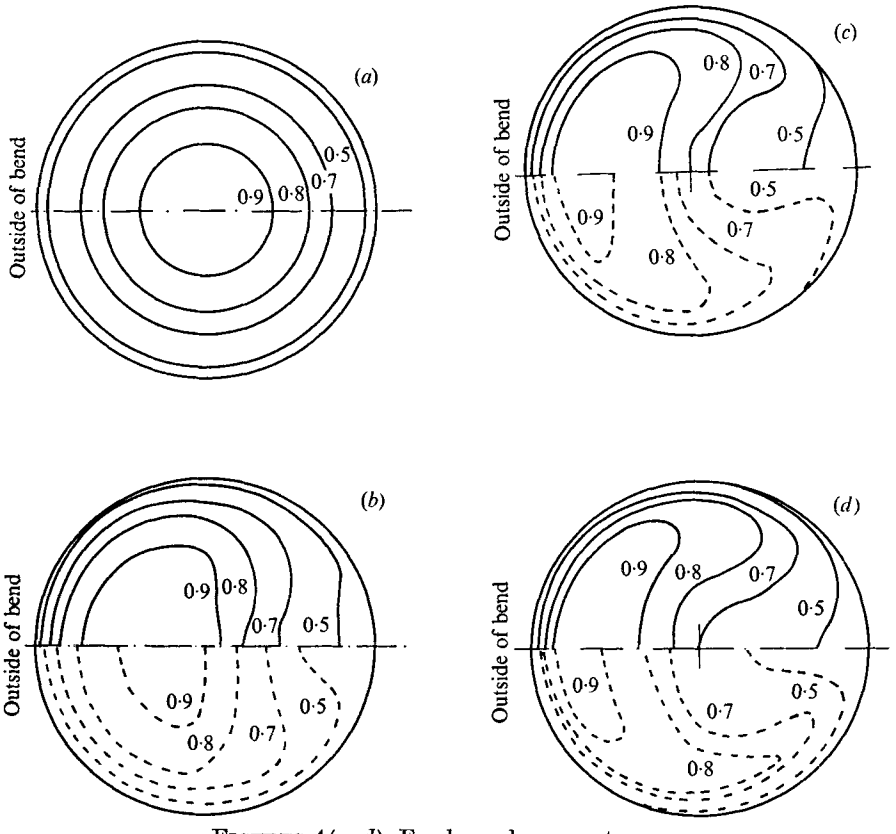


FIGURES 4(*a–d*). For legend see next page.

(4) Since the cross-stream velocities do not satisfy the continuity equation locally, a 'Poisson' equation is derived from this equation and the two linearized cross-stream momentum equations; this Poisson equation is then solved for corrections to the pressure ($p$) field. Thereafter the cross-stream velocities are corrected accordingly.

(5) The kinetic-energy and dissipation equations are solved so as to provide the new distributions appropriate to the downstream station.

(6) A new downstream station is chosen and steps 1–5 are repeated.

In an iterative version of this scheme, which is preferable if large steps are to be taken, the velocities are under-relaxed and operations 1–5 are repeated at the same section, the latest values of the pressure, kinetic-energy and dissipation fields being used at each repetition.

## 3. Results and discussions

### 3.1. *Computational details*

In the computations whose results are reported here, the finite-difference grid possessed 14 intervals in the radial direction and 11 intervals in the $\theta$ direction; the grid covered only a semi-circular sector because the flow must be symmetrical

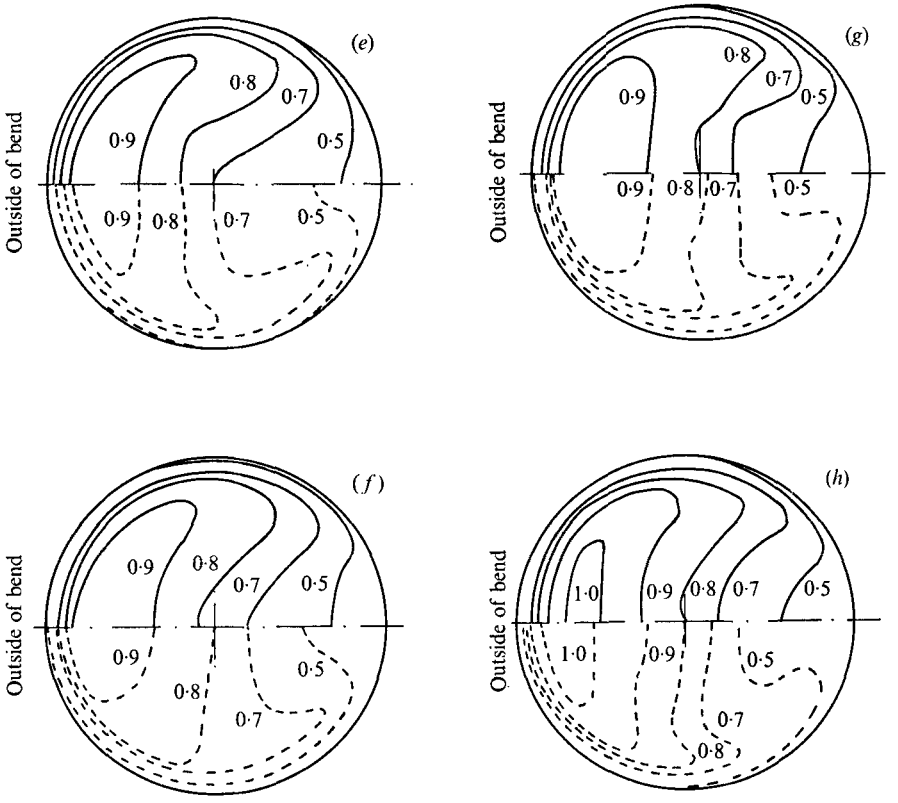


FIGURE 4. Contours of velocity head non-dimensionalized with $\frac{1}{2}\rho U_0^2$; $U_0$ is the centre-line velocity at the inlet. ——, predictions; – – – –, experimental results, Rowe (1966). The Reynolds number of the flow is $2{\cdot}36 \times 10^5$ and $R/a = 24{\cdot}0$. Angular position along bend: (*a*) 0°; (*b*) 30°; (*c*) 45°; (*d*) 60°; (*e*) 90°; (*f*) 120°; (*g*) 150°; (*h*) 180°.

about a diameter passing through the axis of curvature. Some computations were repeated with finer grids; but it was observed that the difference in the solutions was of the order of 2–3%. Therefore a $14 \times 11$ grid was used in all further computations. The forward-step size was decided after similar tests and was fixed to be 1·5°. Between two stations the solution was iterated; each time a more correct pressure field was used for the cross-stream velocities and a more correct axial pressure gradient.

The developing-flow solutions were obtained by this marching procedure with small forward steps; however when only the fully developed flow was computed, very large forward steps were taken and the velocities were under-relaxed at each step. The computer time on a CDC 6600 computer was of the order of 0·45 s per forward step for the present grid, without iteration.

### 3.2. *Presentation of the results*

Figures 4(*a*)–(*h*) provide a comparison of the predicted velocity-head contours with the experimental results of Rowe (1966) for a 180° pipe bend. The Reynolds number of the flow was $2{\cdot}36 \times 10^5$ and the ratio of bend radius to pipe radius was

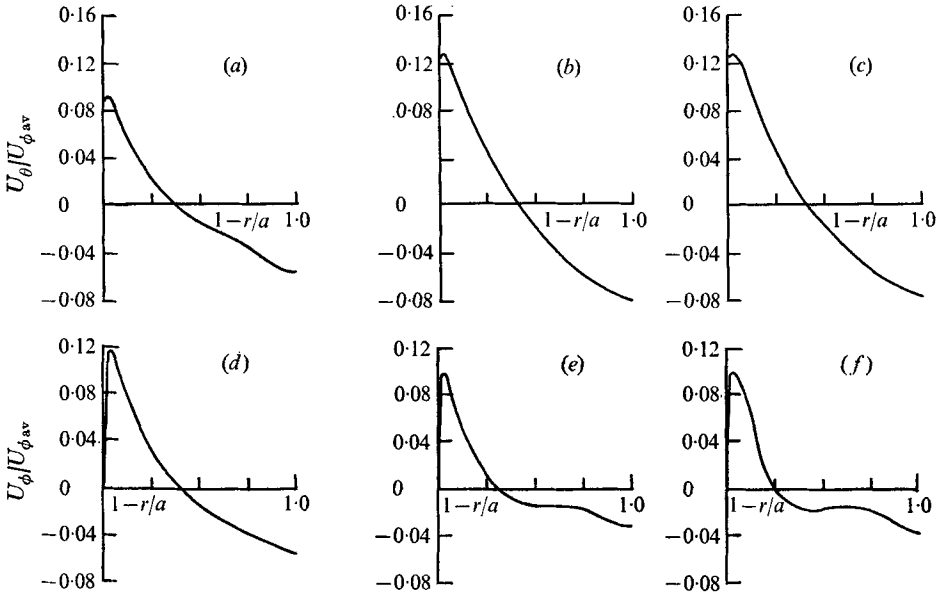


FIGURE 5. Secondary-velocity profiles along a vertical radius in a 180° bend; the flow Reynolds number is $2{\cdot}36 \times 10^5$ and $R/a = 24.0$. Angular position along bend: (*a*) 15°; (*b*) 30°; (*c*) 45°; (*d*) 60°; (*e*) 120°; (*f*) 180°.

24. Comparisons are made for various angular positions along the bend, the flow at the inlet being a fully developed turbulent pipe flow.

It is seen that, both for the predictions and the experiments, the velocity field is distorted with the velocity maximum shifted to the outside of the bend.

The secondary velocities along the vertical diameter are plotted in figures 5(*a*)–(*f*) for various angular positions along the bend. It was observed by Rowe (1966) that the secondary velocities increase up to a distance of 30° and then decrease, owing to the production of streamwise vorticity of opposite sign. The predictions also display such a reduction in the secondary flow.

The agreement of predicted total-velocity contours with measurements is fairly satisfactory; however, since it is not as good as that reported by Patankar *et al.* (1974) for laminar flow, it is probable that the turbulence model is the source of what discrepancies exist.

### 3.3. *Fully developed flow*

Figure 6 displays a comparison of predictions based on the two-equation turbulence model with experimental data (Hogg 1968; Mori & Nakayama 1967) for flow in a helically coiled pipe, at a section far enough from the entry for the pattern of flow not to change from one section to the next. In figure 6(*c*), results are also presented for calculations using a form of the mixing-length hypothesis. It can be seen that the two-equation turbulence model yields superior predictions. The fully developed friction factors are compared with Ito's empirical formula in figure 7. Also presented in figure 7 are the computed friction factors for turbulent flow in straight circular pipes; the agreement with experimental data is

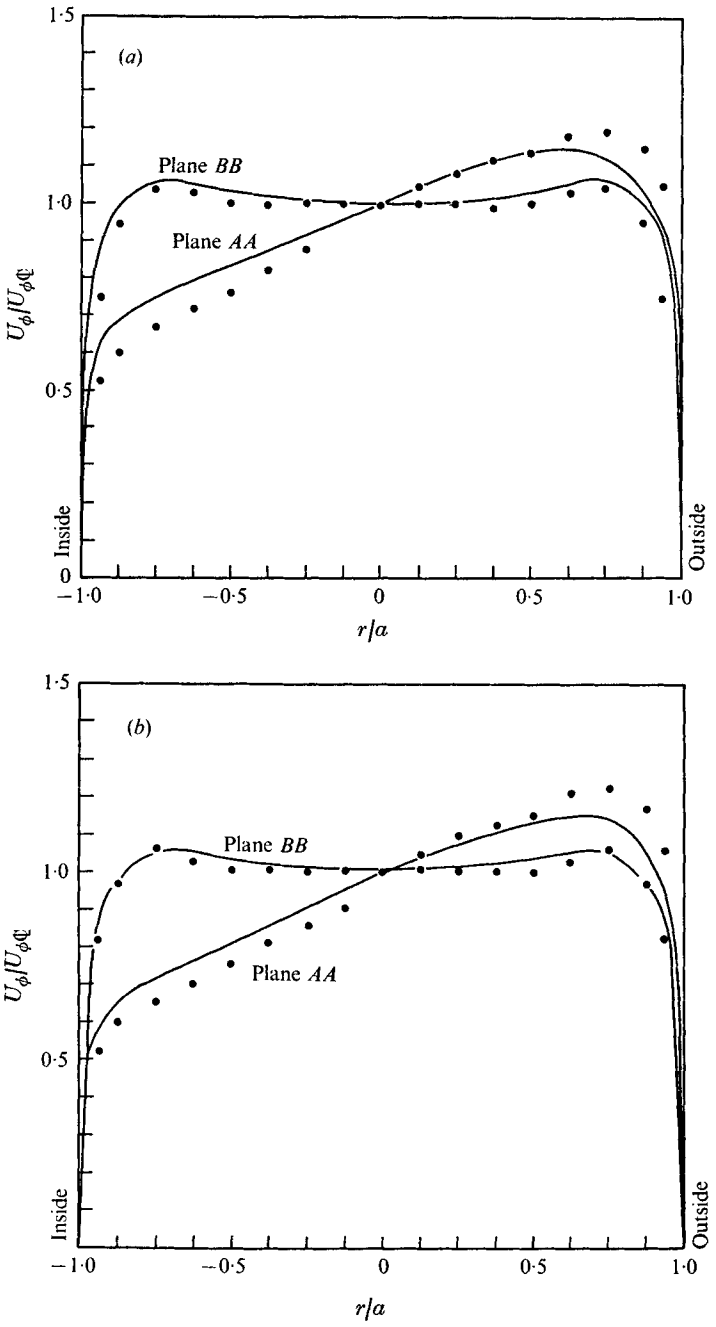


FIGURES 6(*a*, *b*). For legend see next page.

quite satisfactory. However, for the case of curved pipes, the magnitude of the friction factor is underpredicted; the maximum difference between the experimental and computed values is about 8%. This discrepancy confirms the need, pointed out earlier, to refine the turbulence modelling.

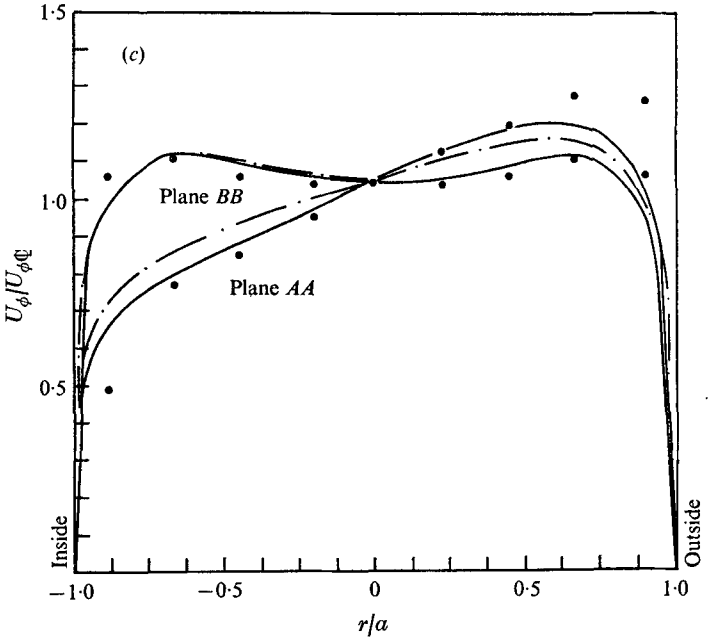


FIGURE 6. Comparison of fully developed axial velocity profiles along planes $AA$ and $BB$. ——, predictions using $k, \epsilon$ model. (*a*) Reynolds number $= 8{\cdot}9 \times 10^4$, $R/a = 25{\cdot}9$; ●, experimental, Hogg (1968). (*b*) Reynolds number $= 6{\cdot}8 \times 10^4$, $R/a = 25{\cdot}9$; ●, experimental, Hogg (1968). (*c*) Reynolds number $= 2{\cdot}5 \times 10^4$, $R/a = 40$; ●, experimental, Mori & Nakayama (1967); —·—, predictions using mixing-length model.

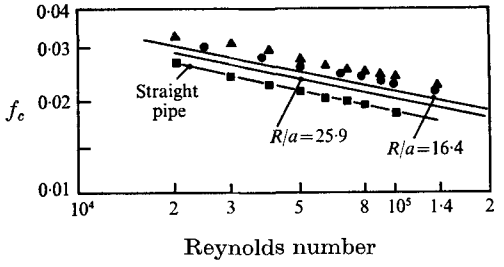


FIGURE 7. Comparison of fully developed friction factors with experimental data. Experimental data: ■, Schlichting (1962); ●, Ito (1959), $R/a = 25{\cdot}9$; ▲, Ito (1959), $R/a = 16{\cdot}4$. ——, predictions using $k$, $\epsilon$ model.

## 4. Conclusions

In the present study, a two-equation turbulence model, incorporated into a numerical solution procedure, has been employed to predict the flow characteristics in a curved pipe. Both developing and fully developed flow regimes were studied. The predictions display reasonable agreement with experimental data and the computation times are modest.

However, the agreement of predictions with the measured data is less good than for laminar flow; therefore the turbulence modelling requires improvement.

Possible modifications are (i) to discard the effective-viscosity approach and to solve differential equations for each individual shear stress, or (ii) to employ an intermediate approach, such as that proposed by Launder (1971), where the differential equations for turbulent shear stresses are approximated by algebraic equations. These tasks are being considered for the future.

## Appendix

*Expressions for the stresses*

The combined laminar and turbulent shear stresses are expressed in the form

$$\tau_{ij} = (\mu_l + \mu_t) D_{ij}, \tag{A 1}$$

where $\{D_{ij}\}$ is the deformation tensor and $\mu_l$ is the molecular viscosity of the fluid (which is assumed constant throughout the pipe cross-section). The expressions for $\tau_{ij}$ can be derived by expanding $D_{ij}$ in the present $(r, \theta, \phi)$ co-ordinate system. They are

$$\tau_{rr} = 2\mu \partial U_r/\partial r, \quad \text{where} \quad \mu = (\mu_l + \mu_t), \tag{A 2}$$

$$\tau_{r\theta} = \mu \left( \frac{\partial U_r}{r \partial \theta} - \frac{U_\theta}{r} + \frac{\partial U_\theta}{\partial r} \right) = \tau_{\theta r}, \tag{A 3}$$

$$\tau_{r\phi} = \left( \frac{\partial U_r}{R \partial \phi} - \frac{U_\phi}{R} \cos\theta + \frac{\partial U_\phi}{\partial r} \right) = \tau_{\phi r}, \tag{A 4}$$

$$\tau_{\theta\theta} = 2\mu (\partial U_\theta / r \partial \theta + U_r / r), \tag{A 5}$$

$$\tau_{\theta\phi} = \mu \left( \frac{\partial U_\phi}{r \partial \theta} + \sin\theta \frac{U_\phi}{R} + \frac{\partial U_\theta}{R \partial \phi} \right) = \tau_{\phi\theta}, \tag{A 6}$$

$$\tau_{\phi\phi} = 2\mu \left( \frac{\partial U_\phi}{R \partial \phi} + \frac{1}{R} (U_r \cos\theta - U_\theta \sin\theta) \right). \tag{A 7}$$

*Expression for generation of kinetic energy*

The expression for $G$ in the $(r, \theta, \phi)$ co-ordinate system is derived from its tensor invariant form. After neglect of small terms, it reduces to

$$G = \mu_t \left\{ 2 \left[ \left( \frac{\partial U_r}{\partial r} \right)^2 + \left( \frac{\partial U_\theta}{r \partial \theta} \right)^2 + \left( \frac{U_r}{r} \right)^2 + \frac{2}{r^2} U_r \frac{\partial U_\theta}{\partial \theta} - \frac{U_\theta}{r} \left( \frac{\partial U_r}{r \partial \theta} + \frac{\partial U_\theta}{\partial r} \right) \right] + \left( \frac{\partial U_r}{r \partial \theta} + \frac{\partial U_\theta^2}{\partial r} \right) + \left( \frac{\partial U_\phi^2}{\partial r} \right) + \left( \frac{\partial U_\phi}{r \partial \theta} \right)^2 + \frac{U_\theta^2}{r^2} + \frac{U_\phi^2}{R^2} + \frac{2}{R} U_\phi \left( \frac{\partial U_\phi}{r \partial \theta} \sin\theta - \frac{\partial U_\phi}{\partial r} \cos\theta \right) \right\}. \tag{A 8}$$

## REFERENCES


Curr, R. M., Sharma, D. & Tatchell, D. G. 1972 Numerical predictions of some three-dimensional boundary layers in ducts. *Comp. Methods in Appl. Mech. & Engng*, **1**, 143–158.

Gosman, A. D. & Spalding, D. B. 1971 The prediction of confined three-dimensional boundary layers. *Salford Symp. on Internal Flows*, paper 19. London: Inst. Mech. Engrs.

Hanjalić, K. 1970 Ph.D. thesis, London University.

Hawthorne, W. R. 1951 Secondary circulation in fluid flow. *Proc. Roy. Soc.* A **206**, 374–387.

Hogg, G. W. 1968 Ph.D. thesis, University of Idaho.

Ito, H. 1959 Friction factors for turbulent flow in curved pipes. *Trans. A.S.M.E., J. Basic Engng*, **82**, 123–132.

Koosinlin, M. L. & Lockwood, F. C. 1974 The prediction of axisymmetrical turbulent swirling boundary layers. *Imperial College, Mech. Engng Dept. Rep.* HTS/73/1.

Launder, B. E. 1971 An improved algebraic modelling of the Reynolds stresses. *Imperial College, Mech. Enging. Dept. Rep.* TM/TN/A/9.

Launder, B. E. & Spalding, D. B. 1972 *Mathematical Models of Turbulence*. Academic.

Mori, Y. & Nakayama, W. 1967 Study on forced convective heat-transfer in curved pipes. *Int. J. Heat Mass Transfer*, **10**, 37–59.

Ng, K. H. & Spalding, D. B. 1972 *Phys. Fluids*, **15**, 20–30.

Patankar, S. V., Pratap, V. S. & Spaldng, D. B. 1974 Prediction of laminar flow and heat transfer in helically coiled pipes. *J. Fluid Mech.* **62**, 539–551.

Patankar, S. V. & Spalding, D. B. 1972 A calculation procedure for heat, mass and momentum transfer in three-dimensional parabolic flows. *Int. J. Heat Mass Transfer*, **15**, 1787–1806.

Rodi, W. & Spalding, D. B. 1970 A two-parameter model of turbulence and its application to free jets. *Wärme & Stoffübertragung*, **35**, 85–95.

Rowe, M. 1966 Some secondary flow problems in fluid dynamics. Ph.D. thesis, Cambridge University.

Runchal, A. K. 1969 Ph.D. thesis, London University.

Schlichting, H. 1962 *Boundary Layer Theory*. McGraw-Hill.

Sharma, D. & Spalding, D. B. 1971 Laminar flow heat transfer in rectangular-sectioned ducts with one moving wall. *1st Nat. Heat & Mass Transfer Conf., India Inst. Tech., Madras*, paper HMT-26-71.

Wolfshtein, M. 1969 Ph.D. thesis, London University.